

# Two-Dimensional Position Detection System with MEMS Accelerometer for MOUSE Applications

Seungbae Lee, Gi-Joon Nam, Junseok Chae, Hanseup Kim, and Alan J. Drake

Department of EECS, University of Michigan

Ann Arbor, MI 48109-2122

seungbae{criteria, jchae, hanseup, ajdrake}@eecs.umich.edu

## ABSTRACT

A hybrid two-dimensional position sensing system is designed for mouse applications. The system measures the acceleration of hand-movements which are converted into two-dimensional location coordinates. The system consists of four major components: 1) MEMS accelerometers, 2) CMOS analog read-out circuitry, 3) an acceleration magnitude extraction module, and 4) a 16-bit RISC microprocessor. Mechanical and analog circuit simulation shows that the designed padless mouse system can detect accelerations as small as 5.3 mg and operate up to 18MHz.

## 1. INTRODUCTION

Most commercial mouse systems are built with rolling-ball or optical technology to provide cursor positions. For example, a ball mouse system detects physical rolling movements of the ball, which are affected by a non-flat or obstructed surface. An optical mouse system avoids these environmental factors by detecting the reflection of light on a reflective supplementary pad. Both technologies, however, require a special surface limiting the working space and freedom of the user's movements. Obviously, a more desirable mouse system would not be restricted by environmental factors.

In this paper, we describe a novel mouse system design which detects two-dimensional positions without any additional components such as pads. Shown in Figure 1, the system consists of four major components: 1) MEMS (Micro Electro Mechanical Systems) accelerometers, 2) CMOS analog read-out circuitry, 3) an acceleration magnitude extraction module, and 4) a 16-bit RISC microprocessor. Two MEMS accelerometer devices are employed to measure  $X$  and  $Y$ -axis acceleration of the movements from the user's hand. These acceleration values are pulse-width modulated by the CMOS analog read-out circuitry and will be converted into  $(X, Y)$  coordinates on the screen by performing integral operations using a 16-bit RISC microprocessor. In this design, we present a hybrid configuration system, which means each component is not based on the same substrate and thus has to be interfaced with each other by means of external connections. The MEMS device is designed in S.O.G. (Silicon On Glass) technology developed at the University of Michigan. The analog readout circuit is designed in a dual-poly, single-metal process, also developed at the University of Michigan and the digital microprocessor is designed in a 1.5  $\mu\text{m}$  AMI process through MOSIS using SCMOS design rules.

The rest of this paper is organized as follows. Section 2 presents the overall system architecture and explains each module in detail. Section 3 describes the verification and testing methodology for our system. Section 4 reports the statistical data of the final design. Sec-

tion 5 describes monolithic implementation of the mouse as future work with conclusion in Section 6.

## 2. SYSTEM OVERVIEW

### 2.1 System Requirements and Constraints

Two system requirements stand out for consideration: *speed* and *accuracy*. Generally the speed of physical reaction from a human is remarkably slow compared to the speed of a modern microprocessor and it is reported that the magnitude of an action is at most on the order of  $10^{-2}$  seconds [1]. Since the mouse system must generate  $(X, Y)$  coordinate values faster than this rate, the target clock frequency was chosen to be 100 kHz, which provides 500 instructions per coordinate calculation. In terms of movement accuracy, the finest acceleration from a human hand is more than 10 mg ( $g=9.8\text{m/s}^2$ ). One of the most important figures of merit in MEMS accelerometers is sensitivity which is defined as the capacitance variation per acceleration change. The capacitance change due to acceleration input is detected and converted to a voltage in analog read-out circuits. Accordingly, together with the MEMS accelerometer's sensitivity, the gain and equivalent input noise of the analog read-out circuits determine the overall minimum detectable acceleration. The analog read-out circuits and MEMS accelerometer are designed to detect acceleration as small as 5 mg so that our system can catch the smallest movement of the human hand.

### 2.2 Design Methodology

A capacitive sensing configuration, as shown in Figure 2, was chosen for the MEMS accelerometer because it gives high sensitivity with low temperature drift [4]. The device dimensions optimize large sensitivity over layout area and its functionality was verified using ANSYS.

For the analog read-out circuit design, switched capacitor circuits were chosen to simplify the interface between the analog and the digital parts. All the analog circuit designs were simulated with HSPICE and laid out using Mentor Graphics software.

A top-down approach was used to partition the design into its various analog, digital, and MEMS components. Each module was verified using a bottom-up approach for timing, functionality, and LVS. The majority of modules—the microprocessor datapath, analog circuitry, and MEMS devices—are full custom designs while the

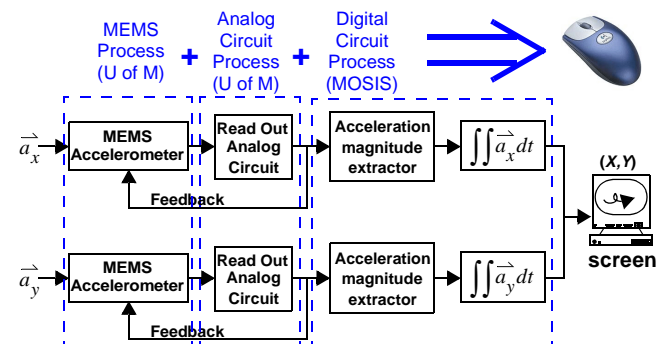


Figure 1. Block diagram for the hybrid MOUSE system.

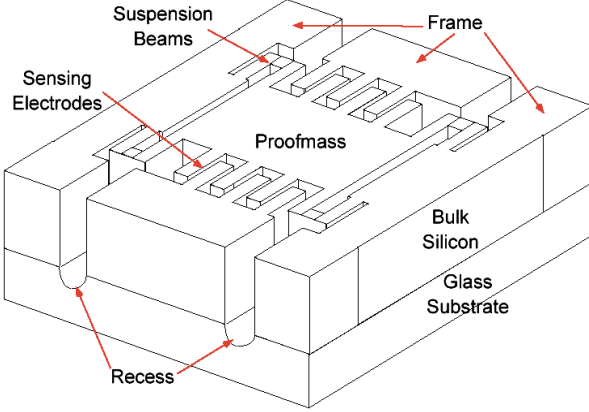


Figure 2. S.O.G MEMS accelerometer.

microprocessor controller was designed using Verilog HDL.

### 2.3 Operational Overview

Figure 1 shows an operational block diagram of the mouse system. When a user moves the mouse in an arbitrary direction, the acceleration is decomposed into *X*- and *Y*-axis acceleration components by a corresponding "MEMS accelerometer". The actual acceleration value is represented by a differential capacitance between two capacitors in the MEMS device. This capacitance value is simultaneously fed back to reset the MEMS device—so the next acceleration can be measured without any bias—and fed forward into the CMOS analog read-out circuitry where it is converted into a digital pulse-width modulated output voltage. The polarity of the pulse, either positive or negative, determines the direction of the acceleration and the width of the pulse is proportional to the magnitude of the acceleration. An "acceleration magnitude extractor" changes the generated pulse width into the units of system clock frequency, which will be used by the microprocessor to calculate the exact position coordinate values on the screen.

### 2.4 MEMS Accelerometer

Typically, there are three different types of MEMS accelerometers, piezo-resistive [2], tunneling [3], and capacitive [4, 5]. The capacitive accelerometer was chosen for this system because it provides high sensitivity, good DC response, low drift, low temperature sensitivity, low-power dissipation, and a simple structure [6]. S.O.G technology was chosen for the implementation, instead of some other technology, to take advantage of its robustness and simplicity of design.

Figure 2 shows the structure of a S.O.G. lateral accelerometer [4]. A MEMS accelerometer consists of two major components: a proof mass and sensing electrodes. A proof mass and sensing electrodes are connected to a frame which is anchored to a glass substrate. Since the proof mass is suspended over a recess on a glass substrate with serpentine suspension beams, it is free to move in response to an external acceleration. Electrodes attached to the glass substrate are stationary. When external forces are applied to the accelerometer (by the user's hand movement, for example), the proof mass moves against the forced direction due to an inertia force while the electrodes remain stationary. The movement causes capacitance variations between the comb fingers which form parallel plate capacitors, denoted as  $\Delta C$ . One side of the comb fingers generates a positive variation ( $+\Delta C/2$ ), and the other side produces a negative one ( $-\Delta C/2$ ). The total capacitance change is the difference between these two values [ $+\Delta C/2 - (-\Delta C/2)$ ]. Therefore, the external acceleration is converted to the differential capacitance variation which can be expressed as:

$$\Delta C(pF/g) = \frac{9.8 \cdot M}{k \cdot d_o} \cdot C_s \quad (1)$$

where  $M$  is the mass of the proof mass,  $C_s$  is the rest capacitance,  $d_o$

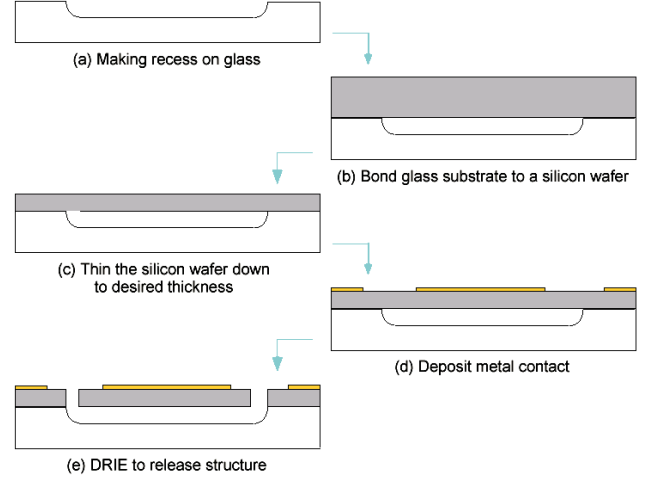


Figure 3. Fabrication process sequence

is the sensing gap distance, and  $k$  is the spring constant of the suspension beams[5]. From Eqn.(1), it can be expected that a heavy accelerometer with a large number of comb fingers and compliant structure—i.e., small spring constant—provides good sensitivity, although it is difficult to fabricate such accelerometers. A single crystal silicon proof mass 2.1 mm wide, 2.4 mm long, and 100  $\mu m$  high gives 0.78 pF/g sensitivity. For the two-dimensional mouse system, two lateral accelerometers are required for sensing *X* and *Y*-axis accelerations. A schematic top view of the MEMS accelerometer in Figure 2 is shown in Figure 5.

The fabrication process has 5 steps requiring only 3 masks developed at the University of Michigan. Figure 3 shows the cross section of the wafer for each fabrication step and Figure 4 shows an SEM (Scanning Electron Microscope) picture of a MEMS accelerometer taken after fabrication.

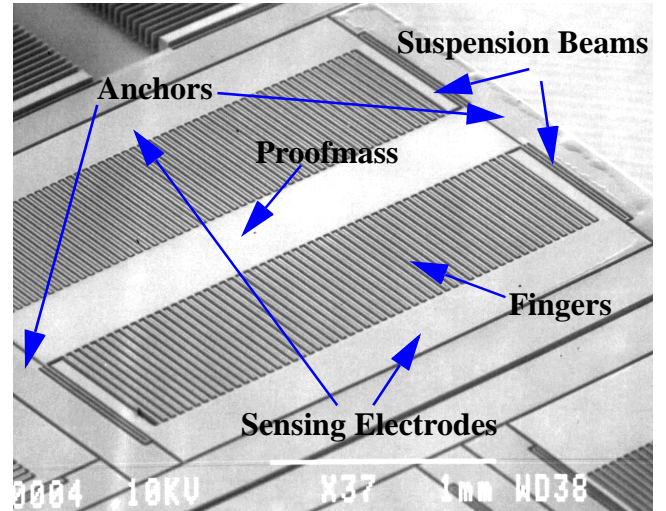


Figure 4. Top view of a MEMS accelerometer.

### 2.5 CMOS Analog Read-Out Circuits

The detected acceleration, which represents a differential capacitance variation from the MEMS accelerometer, is modulated by the analog read-out circuitry shown in Figure 5. In general, the lateral accelerometer presented in Section 2.4 can be operated either in open-loop mode or closed-loop mode. In closed-loop operation the overall performances such as linearity, dynamic range, and band-

width are improved [5]. In our design, an electromechanical over-sampled modulator is used because it provides direct digital output and force feedback control of the proof mass simultaneously over a wide dynamic range.

A switched capacitor front-end, shown in Figure 5 (a), was chosen because it is insensitive to the input parasitic capacitance. An efficient gain and offset compensated integrator is obtained by using an offset-storage capacitor,  $C_o$ , and a correlated double sampling (CDS) technique[7]. This circuit uses a single-ended charge integrator to read out the capacitance variation and the static comparator forms the loop quantizer. Finally, a digital flip-flop samples the output from the comparator and synchronizes its bit stream with the system clock. Since the proof mass can be modeled as a second order system the closed loop system becomes unstable so a simple lead compensator,  $H_c(z)$ , is inserted in the feedback path for stability.

There are four clock phases in the switched-capacitor interface circuit. During the first phase ( $\phi_1$ ) the sense capacitors formed between the electrodes and the proof mass are reset and the Op amp offset voltage is stored on  $C_o$ . In the second phase ( $\phi_2$ ) sense capacitors,  $C_{right}$  and  $C_{left}$  are charged through  $V_+$  and  $V_-$ . The charge difference between  $C_{right}$  and  $C_{left}$  is integrated on the feedback capacitor,  $C_i$ , while the comparator quantizes the charge. In this phase, the offset voltage stored on  $C_o$  is subtracted and thus the output offset voltage of the Op amp is compensated. The amplitude of the Op amp output voltage corresponds to the magnitude of the applied acceleration. For example, if the MEMS device gets positive acceleration, then the proof mass is closer to the left anchor of the MEMS accelerometer and  $C_{left}$  is bigger than  $C_{right}$ . Since  $C_{left}$  is connected to the negative reference voltage ( $V_-$ ), the negative net charge is sampled to an integrator, generating a positive Op amp output voltage. The capacitance sensitivity defined as the Op amp output voltage due to input capacitance change ( $\Delta C$ ) is calculated by:

$$V_o = \left( \frac{\Delta C}{C_i} \right) (V_+ - V_-) \quad (2)$$

From Eqn.(2) the capacitance sensitivity is approximately 0.33 V/pF. The quantized output is also latched at the end of this phase. In the last phase ( $\phi_3$ ) the output of the flip-flop is fed back to the MEMS accelerometer to place the proof mass in the nulling position by electrostatic forces. An additional phase ( $\phi_4$ ) is used for the control and sensing of the proof mass. The output of the latch forms pulse bit streams for the next module.

Figure 6 shows the HSPICE simulation result of the modulation of acceleration magnitudes into the corresponding digital pulse bit streams (PWM signal). The layout for the analog read-out circuit is shown in Figure 7

## 2.6 Noise Analysis of Closed Loop System

There are several noise sources that affect the performance of the overall system; determining the minimum detectable input acceleration. In an oversampled electromechanical sigma-delta system,

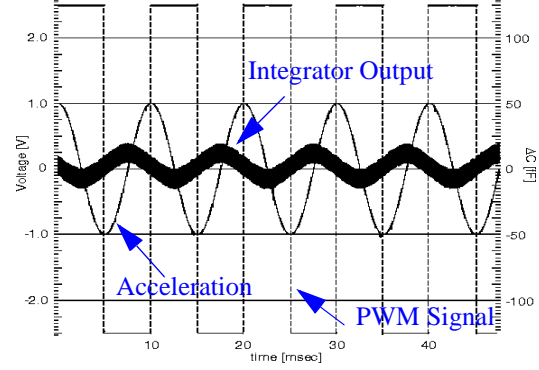


Figure 6. HSPICE simulation for analog read-out circuit.

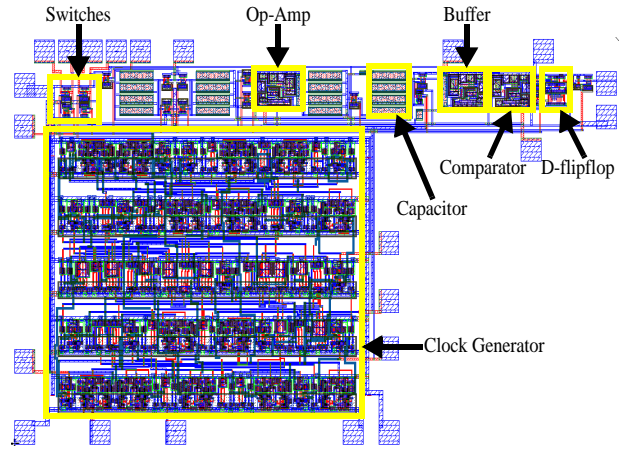


Figure 7. Layout for Sigma-Delta analog readout circuitry. (die size: 4.5mm x 2.6mm)

higher sampling rates reduce the quantization noise and result in a 3 dB signal-to-noise ratio improvement for each doubling of the sampling frequency. Each noise source will now be described.

### • Brownian noise:

The primary mechanical noise source for the device is due to the Brownian motion of gas molecules between comb fingers. The total noise equivalent acceleration (TNEA) [  $m/(s^2 \cdot \sqrt{Hz})$  ] [6] is

$$TNEA = \frac{\sqrt{4K_B T D}}{M} = \sqrt{\frac{4K_B T w_r}{QM}} \quad (3)$$

where,  $k_B$  is the Boltzmann constant,  $T$  is the temperature in Kelvin,

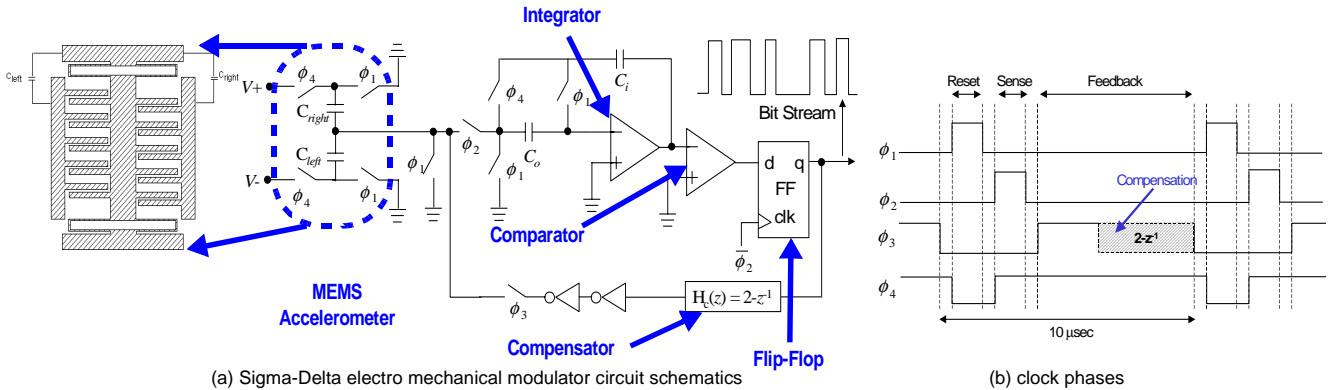


Figure 5. Sigma Delta Electro Mechanical Modulator with clock phases



$D$  is damping coefficient, and  $w_r$  is resonance frequency. From Eqn.(3), it is seen that the MEMS accelerometer has smaller Brownian noise with larger- $Q$  and heavier proof mass. Plugging device data into this equation results in Brownian motion noise around  $10 \mu g / \sqrt{Hz}$ .

#### • Amplifier noise:

The readout circuitry utilizes correlated double sampling to reduce the input CMOS amplifier flicker noise; however, the amplifier thermal noise is amplified by the ratio of total input capacitors, including parasitics in the integrating capacitor. The noise at the output of the amplifier can be expressed by integrating the total noise power and dividing it by the effective noise bandwidth, which is half the sampling frequency. Therefore, the amplifier output noise voltage due to thermal noise in the Op amp is expressed as:

$$V_{Amp-out} = \sqrt{\frac{16}{3} \cdot \frac{C_T}{C_i} \cdot \frac{kT}{C_{out}} \cdot \frac{1}{f_s}} \quad [V / \sqrt{Hz}] \quad (4)$$

where  $C_T$  is the total input capacitance including parasitics,  $C_{out}$  is the capacitance of the Op amp output node, and  $f_s$  is the sampling frequency. From this equation, the equivalent input acceleration noise due to amplifier thermal noise is about  $0.7 \mu g / \sqrt{Hz}$ .

#### • $KT/C$ noise:

A major noise source in switched capacitor circuits is  $KT/C$  noise which is generated by the CMOS switch thermal noise. The rms voltage noise from thermal switch noise can be calculated by the integration of the bandwidth of the switch's RC filter. The voltage noise power density due to this switch thermal noise is expressed as:

$$V_{SC-out} = \sqrt{\frac{kT}{C_i} \cdot \frac{2}{f_s}} \quad [V / \sqrt{Hz}] \quad (5)$$

This  $KT/C$  voltage noise is converted to equivalent input acceleration noise as  $0.3 \mu g / \sqrt{Hz}$ .

#### • Mass residual motion noise:

The proof mass is being rebalanced by a pulse train and thus it has a residual motion with a small ac amplitude. The amplitude of this motion can be shown [8] to be approximately equal to  $\Delta x = 4 a_{max} / (\pi f_s)^2 = 8.0 \times 10^{-9} [m]$  with  $a_{max} = 20g$  and  $f_s = 100kHz$ . This residual motion corresponds to an equivalent rms of  $78 mg$  acceleration in this MEMS accelerometer. This acceleration can be randomized due to the varying input and hence it can be considered to be noise distributed uniformly from dc to the proof mass residual motion frequency  $f_s/4$ . This noise is then equivalent to  $500 \mu g / \sqrt{Hz}$ .

#### • Dead Zone Noise:

Assuming that the input of the accelerometer is zero, the feedback voltage generates  $a_{max}$  with frequency  $f_s/4$  because of electrostatic force. Therefore, the input signal must be large enough to break this dead-zone pattern. The minimum rms input acceleration for this is  $a_{dead-zone} = 8 a_{max} (f_r/f_s)^2 = 160 \mu g$ , and should be counted as noise.

#### • Total noise and Minimum detectable acceleration:

Since all of the noise sources considered here are uncorrelated they may be summed giving a total noise of  $530 \mu g / \sqrt{Hz}$ . Therefore, the minimum detectable acceleration is the same as the one calculated by integrating this input acceleration density over the bandwidth of interest,  $\sim 100 Hz$ . The resultant minimum detectable acceleration is  $5.3 mg$ , which is below the smallest acceleration a human hand can generate/perceive. From the noise source consideration, we see that the mass residual noise dominates with order of magnitude. However, this mass residual motion noise can be significantly reduced by increasing the sampling frequency at the cost of power consumption and complexity.

### 2.7 Acceleration Magnitude Extractor

The modulated pulse bit stream from the CMOS analog read-out circuit is converted into binary data for further processing. Two types of data should be extracted from the pulse bit streams: polarity

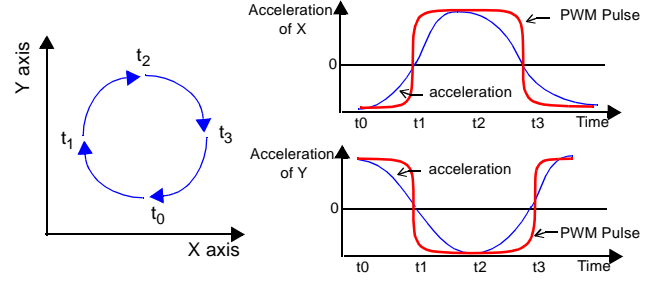


Figure 8. Movements of a mouse and corresponding accelerations in X- and Y-axis.

and magnitude. The polarity indicates the direction of acceleration, and can be handily extracted by observing the sign of pulse bit streams. For example, Figure 8 illustrates the movements of the mouse and corresponding acceleration values on both the X- and the Y-axis. It also shows the possible PWM (Pulse Width Modulation) bit streams. If the value of the pulse is 5 volts (digital value "1"), the acceleration is toward the positive direction, and vice versa. The width of the pulse bit streams is proportional to the magnitude of acceleration. The extraction of correct magnitude of acceleration can be achieved via two binary flags (flip-flops) and a binary counter as shown in Figure 9. The "c" flag is set to the polarity of the current

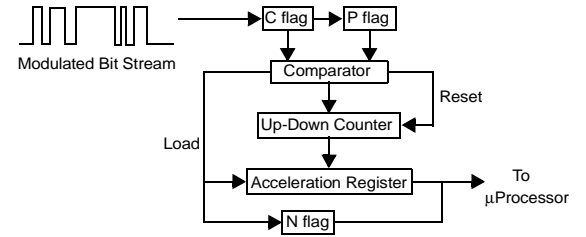


Figure 9. Acceleration Magnitude Extractor.

input pulse bit stream synchronized by the system clock while the "p" flag value is the one shifted from the "c" flag flip-flop in the previous clock cycle. The comparator compares the two flag values and whenever two flag values differ—i.e. the polarity of the input stream changes—it loads the current value of the binary counter into the "acceleration register" and at the same time resets the counter. While the "c" and "p" flags have the same value, the counter keeps increasing or decreasing based on the value of the "c" flag. Thus, the magnitude of generated values is proportional to the degree of the acceleration of movements, and the polarity of the input bit streams determines the direction of the user's movements. The positive value of the counter corresponds to positive acceleration and vice-versa. The "acceleration register" always keeps some static values specifying the previous acceleration magnitude and the control microprocessor only accesses this register to calculate the current position of the cursor. Whenever the acceleration register loads a new value from the counter, the "n" flag is set to "1" indicating that the new value has been loaded. The control microprocessor keeps polling "n" to decide whether it should fetch a new acceleration value or not. The layout of the acceleration magnitude extractor is assembled together with the core microprocessor shown in Figure 11.

### 2.8 Core Control Microprocessor

The core control microprocessor is designed to filter the acceleration output from the analog read-out circuits within the bandwidth of interest and to remove the quantization noise folded at higher frequency as well as other noises. This can be done with a simple FIR low pass filter with  $\sim 100 Hz$  cut-off frequency. Also, the microprocessor calculates the position coordinates based upon the magnitude values of the acceleration from the acceleration extract module. The processor is based on RISC concepts and is implemented as a modified two-stage (fetch/decode and execute) pipeline (Figure 10).

The diagram illustrates the internal components and data flow of a 16-bit RISC processor. It is divided into two main functional blocks: **FETCH** and **EXECUTE**.

- FETCH Stage:**
  - The **PC** (Program Counter) provides the address to **Instruction Memory** and the **Acceleration Registers ( $A_a, A_r$ )**.
  - Instruction Memory** outputs the instruction to the **Instruction Register**.
  - The **Instruction Register** outputs the instruction to the **Decode** block and the **Register File**.
  - The **Register File** outputs the register values to the **Acceleration Registers** and the **Data Memory**.
- EXECUTE Stage:**
  - The **Acceleration Registers** output to the **Register File** and the **Data Memory**.
  - The **Register File** outputs to the **ALU** and the **Shifter**.
  - The **ALU** and **Shifter** outputs are combined with the **PC** output to form the **PC Screen** output.

tion is decoded to allow a full half-cycle for instruction memory access and a full cycle for decoding the instruction. The microprocessor uses a 16-bit word and address space and all instructions are single word. In addition to the basic arithmetic and logic operations, two application specific instructions are implemented which will be described below.

The transferred acceleration magnitude value should be integrated twice so that it is transformed into position coordinates as shown in the following equation:

$$\dot{\vec{v}} = \int_{t_1}^{t_2} (\ddot{a}) dt, \quad \dot{\vec{p}} = \int_{t_1}^{t_2} (\dot{\vec{v}}) dt = \iint_{t_1}^{t_2} (\ddot{a}) dt \quad (6)$$

The other special instruction is called SROUT which moves calculated coordinate values to the 16-bit system interface bus. To minimize the interface with outside circuitry, instruction memory (ROM) as well as data memory (RAM) have been integrated into the core microprocessor module. Both ROM and RAM are 256 words which, due to the simplicity of application program, is big enough to contain the entire application program.

Verification and simulation were performed using the Mentor Graphics Tools and Epoch Design Compiler. Mentor's Quicksim Pro was used for transistor level and Verilog simulation. Parasitics were extracted from the layout, and Mentor's Accusim used for the detailed delay and loading effects. Timing information from the parts generated in Epoch [9] was extracted automatically during the import process to Mentor's Design Architect. Once the functional models were properly back annotated, timing verification was performed in Quicksim Pro. In order to verify the physical design, full mask LVS was performed by importing the custom datapath into Epoch and generating a netlist for the entire core that included the custom and Epoch-synthesized parts.

register value to 16 bit output pins (SOUT[15:0]) allowing us to observe any arbitrary register values of the register file during the testing mode. These hardware features provide ways of testing the ROM, RAM, internal registers, and logic circuits.

The MEMS accelerometer was designed to have a sensitivity of 0.78 pF/g with dimensions of 2.1mm x 2.4mm x 100  $\mu$ m (W x L x H) and a sensing capacitance of 16.4 pF. The analog circuit has estimated power of 3 mW, capacitance sensitivity of 0.3 V/pF, and die size of 4.5mm x 2.6mm. Mechanical and analog simulation shows that the designed padless mouse system can detect acceleration as small as 5.3 mg, which is a high enough resolution for mouse applications.

## 5. MONOLITHIC IMPLEMENTATION

The hybrid two dimensional position detection system has been proposed to combine MEMS accelerometers and digital circuits by means of switched capacitor circuits using wire bonding. Due to the wire bonding, however, these different modules in a system must interface with each other at board level. This not only limits the size of a system, but also contributes capacitive or resistive parasitics that may degrade the system performance[10]. To circumvent these drawbacks of a hybrid system, a system-on-chip (SoC) design and fabrication, where all the modules are fabricated in single wafer, are considered as a monolithic implementation. In other words, all the necessary modules such as MEMS accelerometers, the analog read-out circuit and the microprocessor are to be integrated on the same wafer without any interfaces between them. The only major interface with outside circuits -other than VDD, GND, clock and reset

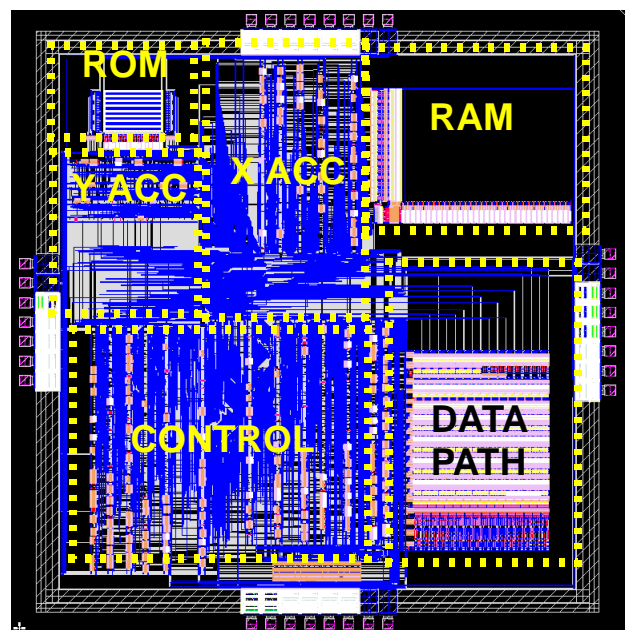


**Figure 11. Microprocessor layout. (5.6mm x 5.8mm)**

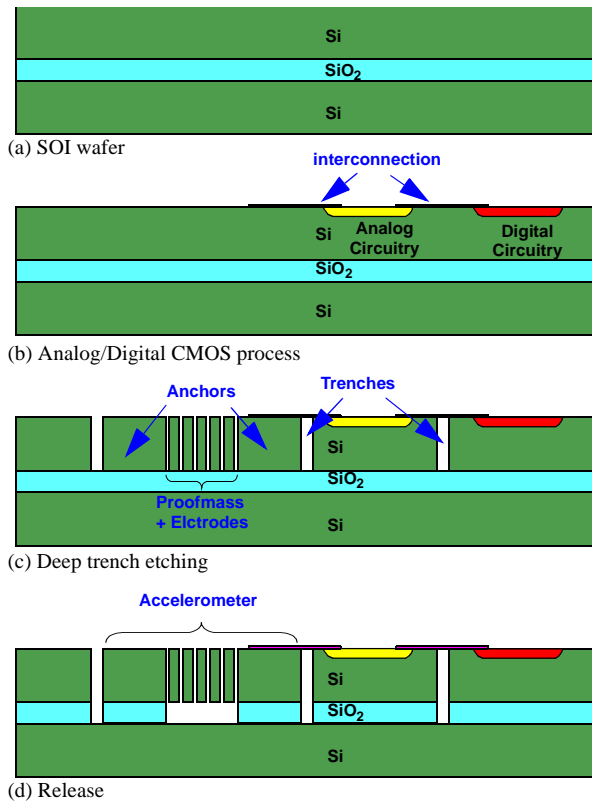


**Figure 12. Process flow of monolithic implementation.**

signals- is the parallel data bus which transfers positional coordinates calculated from the microprocessor. Since they are fabricated on the same wafer, it greatly reduces the overall costs as well as complex steps for the interface. With all these advantages over hybrid system, however, monolithic system has several problems such as noise between analog and digital circuits, interconnections between MEMS devices and analog circuits, and so on. One of the main factor for a noise problem in a monolithic system stems from the fact that the analog and digital circuits are sharing the same substrate. Although substrate has high resistance, it is not a complete isolator and thus voltage variations in digital parts are capacitively coupled to analog circuits and thus may cause malfunctions of a system.

This noise problem due to the substrate coupling can be solved by using Silicon-on-Insulator (SOI) which isolates one module from the other by etching the substrate boundaries of each module and making it isolated both physically and electrically. And more, MEMS accelerometers and analog circuitry can be connected to each other by making deep trenches. It is reported that the silicon substrate underneath interconnection materials such as metals can be removed in the process of deep trench etching because of a sidewall etching effect [11]. The detailed fabrication process flow for monolithic implementation combining MEMS devices, analog and digital circuits are basically post CMOS fabrication, presented in Figure 12. The usual CMOS processes are done using SOI start-wafer as shown in Figure 12(a) and (b). After CMOS processes, deep trenches are made for the formation of proofmass of MEMS accelerometer as well as isolation between analog and digital circuitry as given in Figure 12(c). Figure 12(d) presents the release step by removing SiO<sub>2</sub> with BHF to suspend the proofmass. During release, the SiO<sub>2</sub> between analog/digital circuitry are also etched away. Figure 13 shows the mask level MEMS structure. Close-up view shows a interconnection line, contacts, suspension beams, and etch holes which help releasing proofmass during BHF etch process.

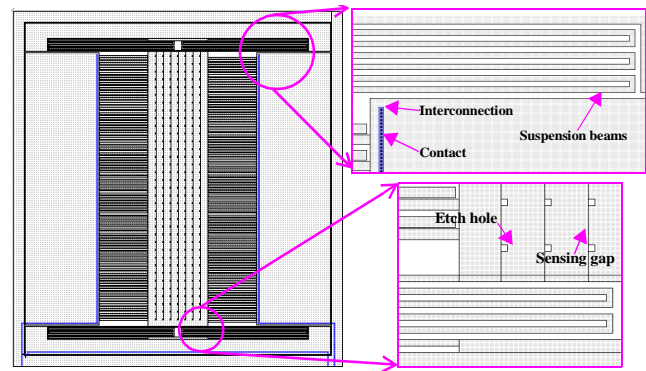


**Figure 13. MEMS accelerometer for monolithic**

## 6. CONCLUSION

In this paper, we presented a novel two-dimensional position detection system for padless mouse applications that do not require any contacts for proper mouse operation. The design requirements were carefully examined and the systematic design methodology was established. The final system consists of four major components: 1) MEMS accelerometer, 2) Analog read-out circuit, 3) Acceleration magnitude extraction module and 4) 16-bit RISC microprocessor. Each module was carefully designed, laid out, and verified through extensive simulation. The calculated and simulated minimum detectable acceleration is 5.3 mg.

The hybrid multi-chip nature of the proposed system will limit the system size and contribute capacitive and resistive parasitics that may degrade the system performance. To circumvent these drawbacks, a system-on-chip (SoC) design and fabrication, where all the modules are fabricated on a single wafer, are considered as future work in this area. Also, the system can be handily extended into a three-dimensional position detection system by adding an additional MEMS accelerometer to measure Z-axis directional movement.

## REFERENCES

- [1] <http://bioen.okstate.edu/Home/fharry/4212/HUMAN.PP.HTM>
- [2] L. M. Roylance and J. B. Angell, "A batch-fabricated silicon accelerometer," *IEEE Trans. Electron Devices*, vol. ED-26, pp.1911-1917, Dec. 1979.
- [3] C. Yeh and K. Najafi, "A low-voltage bulk-silicon tunneling based microaccelerometer," *Tech. Dig. IEEE IEDM*, Washington, DC. Dec. 1995. pp.593-596.
- [4] J. S. Chae, H. Kulah, K. Najafi, "A High Sensitivity Silicon-On-Glass Lateral  $\mu$ G Microaccelerometer," *Nanospace '2000*, Houston, TX.
- [5] N. Yazdi, K. Najafi, "An All-Silicon Single-Wafer Fabrication Technology for Precision Micro Accelerometers", *Proc. Transducers 97*, pp. 1181-1184.
- [6] N. Yazdi, F. Ayazi, and K. Najafi, "Micromachined inertial sensors", *Proc. of the IEEE*, Vol 86, pp.1640-1659, Aug 1998.
- [7] Christian C. Enz and Gabor C. Temes, "Circuit Techniques for Reducing the Effects of Op-Amp Imperfections: Autozeroing, Correlated Double Sampling, and Chopper Stabilization", *Proc. of the IEEE*, vol. 84, No.11, Nov. 1996
- [8] B. Boser and R.T. Howe, "Surface Micromachined Accelerometers", *IEEE J. Solid-State Circuits*, vol.31, no.3, pp.366-375, March 1996.
- [9] Epoch, *Epoch: Online Manuals*, Cascade Design Automation Corporation, Online, 1994.
- [10] Weste, N.H.E. and K. Eshraghian, *Principles of CMOS VLSI Design: A System Perspective*, 2nd ed., Addison-Wesley Publishing Company, Massachusetts, 1993.
- [11] H. Xie, et al., "Post-CMOS Processing for High-Aspect-Ratio Integrated Silicon Microstructures", *Proc. Solid-State Sensor and Actuator Workshop 2000*, Hilton Head, pp. 77 - 80.